Experimental test of the quantum-mechanical image-force theory

A. Hartstein, Z. A. Weinberg, and D. J. DiMaria
IBM Thomas J. Watson Research Center, Yorktown Heights, New York 10598
(Received 28 January 1982)

Both photon-assisted-tunneling and internal photoemission measurements have been made on the same metal-oxide-semiconductor samples. The effective barrier heights between the metal (Al or Au) and the oxide (SiO_2) extracted from the internal photoemission measurements are found to be larger by $\sim$0.3 eV than the effective barrier heights extracted from the photon-assisted-tunneling measurements. Only the quantum-mechanical image-force theory is capable of explaining this result.

I. INTRODUCTION

Photon-assisted-tunneling measurements have demonstrated that the classical image-force theory does not provide the proper description of the interaction between tunneling electrons and the metal from which they emerge.[1,2] Internal photoemission measurements, on the other hand, have long been interpreted in terms of the classical image force.[3,4] A qualitative explanation of these seemingly contradictory results has been given in terms of a quantum-mechanical formulation of the image-force problem.[5] The quantum-mechanical image-force theory was then shown to be qualitatively consistent with both photon-assisted-tunneling and internal photoemission measurements.[6] The purpose of this study was to test the quantitative fit of the quantum-mechanical image-force theory with both the photon-assisted-tunneling experiments and the internal photoemission experiments by doing accurate measurements on the same samples. In particular, we wanted to explore the theoretical prediction[6] that the effective barrier heights between the metal and insulator derived from the two experiments would differ by about 0.2 eV.

The physical situation which we are considering for both the experiments and the theoretical calculations is illustrated in Fig. 1. The conduction-band edge (E_c) in the insulator (SiO_2) and the Fermi energy (E_F) in the metal (Al or Au) are shown. The triangular shape for the potential is the result of an applied electric field F. The image-force potential is not shown. Photon-assisted tunneling involves the photoexcitation of an electron by an energy $h\nu_1$ less than the barrier height and the subsequent tunneling of the electron through the barrier. Internal photoemission involves the photoexcitation of an electron by an energy $h\nu_2$ greater than the barrier height and the subsequent transmission of the electron over the barrier. The current measured in a particular experiment is the sum of the contributions from all of the electrons incident on the barrier. From this brief introduction it is clear why a single unified theory is necessary for the description of both processes.

In this paper we report the experimental study of both the photon-assisted tunneling and the internal photoemission at the Al-SiO_2 and the Au-SiO_2 interfaces. These experiments are described in detail in Sec. II. The main result is that the effective barrier heights extracted from the internal photoemission measurements are $\sim$0.3 eV larger than the effective barrier heights extracted from the photon-assisted-tunneling measurements. This is in agreement with the quantum-mechanical image-force theory. In Sec. III both the classical and quantum-mechanical image-force theories are reviewed, and some new numerical results are presented. In Sec. IV the theories are compared

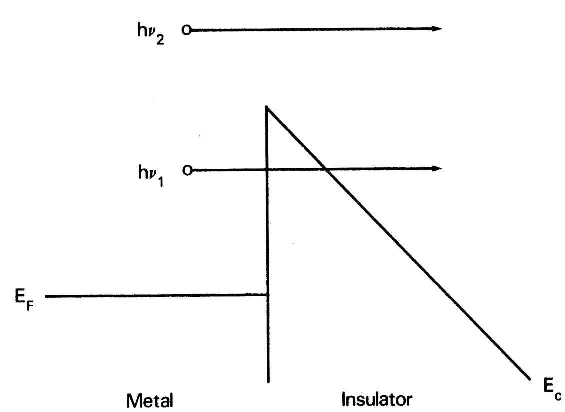

FIG. 1. Electronic structure of the interface illustrating electrons both tunneling through the interfacial barrier ($h\nu_1$) and passing over the barrier ($h\nu_2$) following photoexcitation. E_F is the Fermi energy in the metal and E_c is the conduction-band edge in the insulator.

to experiment and the results are discussed. It is found that the quantum-mechanical image-force theory gives the best description of the experimental results. However, the theory in its present form is not capable of complete quantitative agreement with all aspects of the experimental observations.

II. EXPERIMENT

The samples used in this study were metal-oxide—semiconductor (MOS) capacitors formed on ⟨100⟩-oriented 1-Ω cm *p*-type silicon wafers. Oxides were thermally grown at 1000 °C in a dry oxygen ambient and annealed in nitrogen. The oxide thicknesses were 301 Å for the Al sample and 209 Å for the Au sample. These thicknesses were chosen to minimize the effects of optical interference in the MOS structure and at the same time to minimize the dark currents in the devices. The capacitors were formed by evaporating 0.5-mm metal dots on the oxides. The semitransparent Al dots were 135 Å thick, and the semitransparent Au dots were 200 Å thick.

We studied two wafers with Al counter electrodes and one wafer with Au counter electrodes. Several samples were studied on each wafer, and measurements were made on samples prepared both with and without post-metal anneals. Quantitative differences in the measurements were seen for the different sample treatments. The effect of post-metal anneal on internal photoemission measurements has already been studied.[7] A less detailed account of the effects of sample preparation on photon-assisted-tunneling measurements has also been given.[2] In this paper we seek to test the various theories of photon-assisted tunneling and internal photoemission. Therefore, we made all of our measurements on one sample, and then repeated the procedure several times. Variations from sample to sample were observed in the barrier heights and dielectric constant but the general trends discussed below were the same for all samples.

The physical arrangement for the experiments is shown schematically in Fig. 2. Monochromatic light is incident on the MOS sample from either a laser or a monochromator. The current is then measured as a function of applied voltage both with light on and off. The difference between these two values is the photocurrent. The photoyield is then determined by normalizing the current to the number of photons absorbed in the metal gate. This involves correcting for the source intensity (laser or monochromator), the absorption spectrum of the metal, the photon energy, and the interference of the incident light in the MOS structure. All of the data were normalized in this manner.

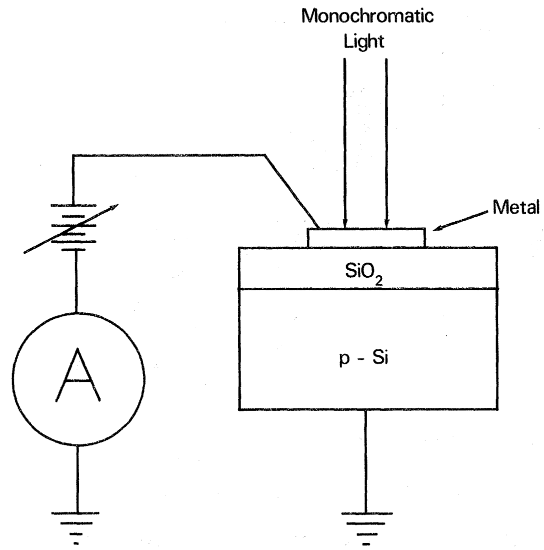

FIG. 2. Schematic representation of the experimental arrangement. Monochromatic light is incident on the MOS sample. The resulting photocurrent is measured using a sensitive picoammeter.

The photon-assisted-tunneling measurements were performed using an argon laser. The experimental technique has been discussed in some detail previously.[1,2] A prism was used to disperse the laser light to filter out any unwanted wavelengths present in the laser beam. For the case of the Al samples four wavelengths in the visible were used. They were 514.5, 488.0, 476.5, and 457.9 nm. For the Au samples two ultraviolet wavelengths of the argon laser were used. They were 363.8 and 351.1 nm.

The data for one of the Al samples are shown in Fig. 3 and the data for Au are shown in Fig. 4. The data are plotted on a standard Fowler-Nordheim tunneling plot. The wavelengths of the incident light for each curve is indicated in the figures. The solid curves represent a one-parameter fit for each set of data. The theory used was the Fowler-Nordheim tunneling theory which neglects image force.[1] For the range of photon energies used, that theory is equivalent to the quantum-mechanical image-force theory because the quantum-mechanical image force becomes negligibly small in the tunneling regime. The parameter in the fit is the barrier height between the ap-

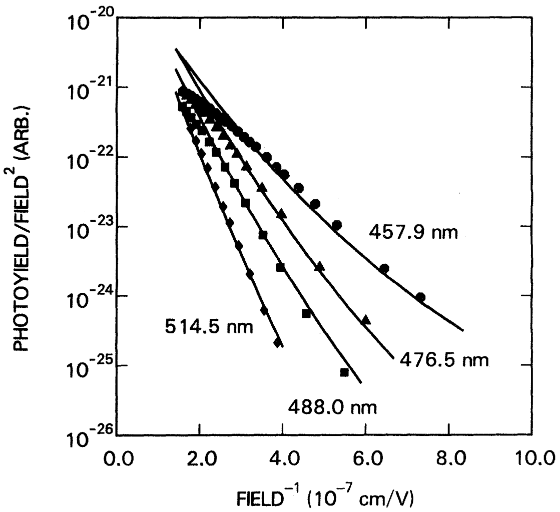

FIG. 3. Photon-assisted-tunneling characteristics of the Al-SiO_2 interface. Each curve is for a different laser wavelength. The solid curves are the theory and the points are the experimental data.

propriate metal and the SiO_2 conduction-band edge. For the Al sample shown the barrier was $\phi=3.25\pm0.01$ eV, and for the Au sample the barrier height was $\phi=3.91\pm0.01$ eV.

The deviations of the data from the theory at high electric fields are observed for non-post-metal-annealed samples but not for the annealed samples used previously.[1] However, the internal photoemission measurements which will be discussed below give better results on unannealed samples.[7] Therefore, we chose to use the samples, unannealed, which would yield the best results on the most difficult part of our experiments, namely the internal photoemission measurements. Whatever uncertainties arise in the barrier determinations from these photon-assisted-tunneling measurements, they are small compared to the uncertainties in the barriers measured by internal photoemission as discussed below. Our choice of samples then minimizes the overall uncertainties in the experiments.

The internal photoemission measurements were performed using a monochromator system described elsewhere.[7] The data obtained for an Al sample are shown in Fig. 5. The data obtained for a Au sample are shown in Fig. 6. These are standard plots for internal photoemission measurements and show the same qualitative features which have been seen many times before. The parameters on the curves are the applied voltages for each curve. Only a portion of the data is displayed so as not to crowd the figures.

We analyzed these data in the conventional way utilizing the classical image-force theory. That theory gives[4]

$$I(h\nu,F)\propto(h\nu-\phi_B+KF^{1/2})^2\ , \tag{1}$$

where I is the photocurrent, $h\nu$ is the photon ener-

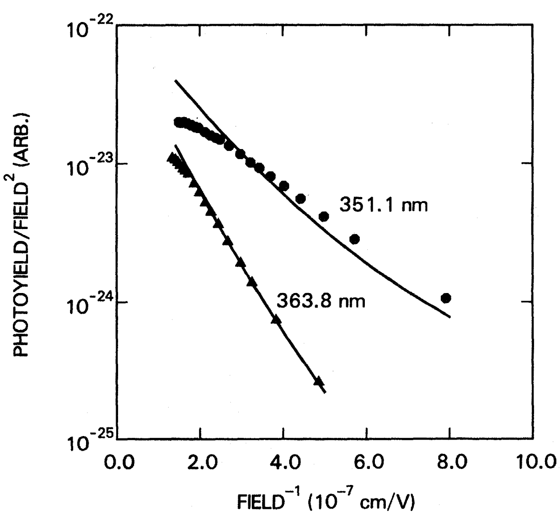

FIG. 4. Photon-assisted-tunneling characteristics of the Au-SiO_2 interface. Two laser wavelengths are shown. The solid lines are the theory and the points are the experimental data.

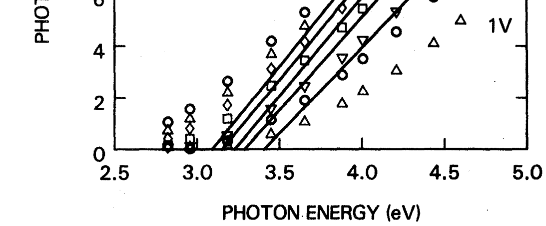

FIG. 5. Internal photoemission characteristics for an Al-SiO_2 interface. The points are experimental data and the solid lines are the extrapolations made to zero photoyield. Each curve is labeled by the voltage applied to the device. Extrapolations were not made for the lowest voltages where the errors in extrapolation would be the largest.

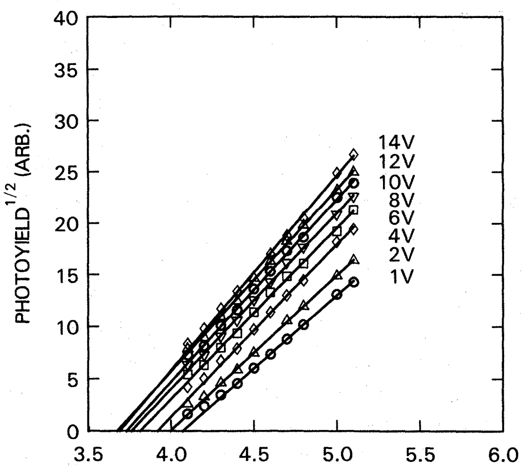

FIG. 6. Internal photoemission characteristics for a Au-SiO_2 interface. The points are experimental data and the solid lines are the extrapolations made to zero photoyield. Each curve is labeled by the voltage applied to the device.

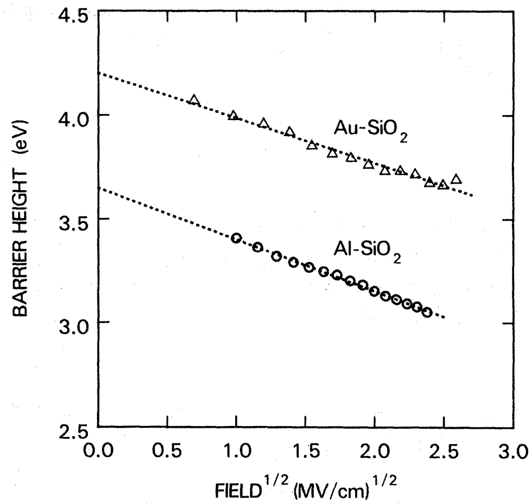

FIG. 7. Effective barrier heights as a function of applied electric field. The circles are for Al and the triangles are for Au. The dotted lines are linear fits to the data. The extrapolation of the curves to zero field is the effective barrier height of the interface, and the slope of the curves is related to the dielectric constant of the insulator.

gy, F is the applied electric field, ϕ_B is the interface barrier energy, and K is a constant. The experimentally determined electric field F is given by $F=(V-\phi_{\rm ms})/d_{\rm ox}$, where V is the applied voltage, $\phi_{\rm ms}$ is the contact potential difference between the appropriate metal and the Si substrate, and $d_{\rm ox}$ is the oxide thickness.

Using this theory, we extrapolated the straight line portion of the curves in Figs. 5 and 6 to zero yield and determined the barriers $\phi(F) =\phi_B-KF^{1/2}$. This extrapolation is clearly an important step in the data analysis. Since all of the theories predict a linear range at high photon energy and a tail at low energy, we extrapolated only the linear portion of the data at high photon energies as shown in the figures. The numerical results of the theories were also extrapolated in the same way. We then plotted these barriers as a function of $F^{1/2}$. The extrapolations of these lines to zero field give the barrier heights derived from the internal photoemission measurements. Figure 7 shows these curves for the Al and Au samples. The barrier height determined in this way for the Al sample is $\phi_B=3.6$ eV, and for the Au sample the barrier height is $\phi_B=4.2$ eV. The average difference between these barriers determined from internal photoemission measurements and the corresponding barriers determined from photon-assisted-tunneling measurements was found to be ~ 0.3 eV.

It must be emphasized that the barrier heights determined in this manner from the internal photoemission measurements are sensitive to which portion of the data is fitted linearly. For example, if more of the lower energy points were included in the fit for the Al data in Fig. 5, a barrier height as low as ~ 3.2 eV could be extracted, which is within the range of values usually found in the literature. In order to accurately compare theory and experiment, we have extrapolated the more easily recognized linear portions of both the experimental and theoretical curves rather than making an arbitrary extrapolation, which includes the curved portions of the data, as has been done in the past. For this reason, our quoted values of the barrier heights derived from internal photoemission are somewhat higher than values found in the literature.

The slopes of the curves in Fig. 7 are the constant K in the classical theory. The slope is related to the dielectric constant of the insulator by the expression $K=(e^3/4\pi\epsilon_0\epsilon)^{1/2}$, where ϵ_0 is the dielectric permittivity of free space, and $\epsilon=2.15$, the optical dielectric constant of SiO_2. From the data shown we find values of $\epsilon=2.3$ for the Al-SiO_2 interface and $\epsilon=3.1$ for the Au-SiO_2 interface. Even wider variations in the values of ϵ have been reported when different processing conditions have been studied.[7] We will have more to say on this subject in the later sections, but the determination of ϵ both experimentally and theoretically is the weakest part of our results and quantitative comparisons are difficult at best.

III. THEORY

The arguments which lead to the formulation of the quantum-mechanical image-force potential have been given in Ref. 5. The calculation which gives the numerical results that can be compared to the internal photoemission and photon-assisted-tunneling measurements has been given in Ref. 6. In this section we review that theory and present the results which pertain to the present experiments.

We consider the problem of an electron in a metal which is incident on the interface with an insulator. What we ultimately want to calculate is the transmission probability of the electron through the interface. The wave function of the electron is denoted by $\psi(x,t)$. We want to describe the interaction between this electron and the remaining electrons in the metal as the electron attempts to tunnel into the insulator. Since all of the electrons move on the same time scale, a Hartree-Fock—type description is adopted. Therefore, the wave function of the incident electron must be adjusted self-consistently to the wave function of the plasma. The wave function of the plasma in this approximation becomes an image of that portion of the wave function of the incident electron which is in the insulator. The image-force potential is then derived from the force on a test charge in the insulator and is given by[5]

$$V_{\rm im}=-\int_0^\infty \left[\frac{e^2\,|\psi(x',t)|^2}{8\pi\epsilon_0\epsilon(x+x')}\right]dx' , \qquad (2)$$

where ϵ_0 is the dielectric permittivity of free space, ϵ is the dielectric constant of the insulator, and x is the distance of the test charge from the interface. A similar result has been derived rigorously for the case where the image force arises from the interaction of an external electron with the surface optical phonons of a dielectric medium.[8]

This potential must now be inserted into the Schrödinger equation in order to calculate the transmission of the interface. This is a very difficult problem, hence we make an important simplifying assumption. We approximate the square of the wave function of the incident electron as a δ function,

$$|\psi(x,t)|^2=\delta(x'-x,t) .$$

After the electron interacts with the barrier, the square of the wave function in the insulator will be $T\delta(x'-x,t)$, where T is the self-consistent transmission of the barrier. This approximation is good as long as the portion of the electron wave function in the insulator remains well localized after it interacts with the barrier. The image-force potential is then given by

$$V_{\rm im}=-Te^2/16\pi\epsilon_0\epsilon x , \qquad (3)$$

i.e., it is the classical result scaled by the transmission of the barrier. For energies far above the top of the barrier, where the electron can be assumed to be a point charge, $T\approx 1$ and Eq. (3) reduces to the classical result. Far below the top of the barrier $T\approx 0$, and the image force is negligibly small. Equation (3) is thus an approximation for the important region near the top of the barrier.

The complete potential which an electron sees in the barrier region is then given by

$$V=\phi_B-eFx-Te^2/16\pi\epsilon_0\epsilon x , \qquad (4)$$

where the first term gives the energy difference between the conduction-band edge of the insulator and the Fermi level of the metal, the second term is the potential in the applied electric field, and the last term is the image-force potential. The transmission of the interface is then calculated by a numerical integration of the Schrödinger equation across the interface, iterating until a self-consistent solution is obtained.

In Fig. 8 we show the transmission probability of an Al-SiO_2 interface for an applied electric field of 5×10^6 V/cm. The figure shows the transmission probability as a function of electron energy. The three curves shown are calculated for the classical image force, the quantum-mechanical image force, and for no-image force. In each case the transmission probability changes abruptly near the barrier height (3.25 eV). It is clear that the results of the quantum-mechanical image-force model approach the results of the classical image-force model for large energy, and approach the results of the no-image-force calculation for small electron energy.

The current measured in an experiment is obtained by summing the transmission probabilities for the incident electrons over the supply function in the metal. The supply function gives the number of electrons incident on the barrier with a particular perpendicular component of momentum. The expression for the current becomes[9]

$$I(h\nu,F)=A\int_{-\infty}^{\infty} S(E,h\nu)T(F,E)dE , \qquad (5)$$

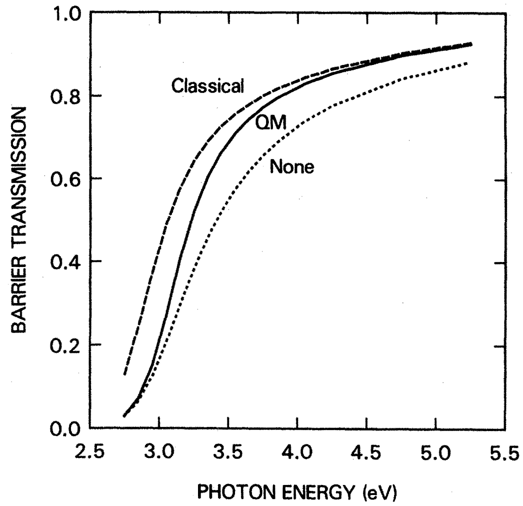

FIG. 8. Barrier transmission probability for an Al-SiO_2 interface calculated for an applied electric field of 5×10^6 V/cm. The barrier occurs at an energy of 3.25 eV. The solid curve is for the quantum-mechanical image-force potential, the dashed curve is for the classical image-force potential, and the dotted curve is for the potential with no image-force included.

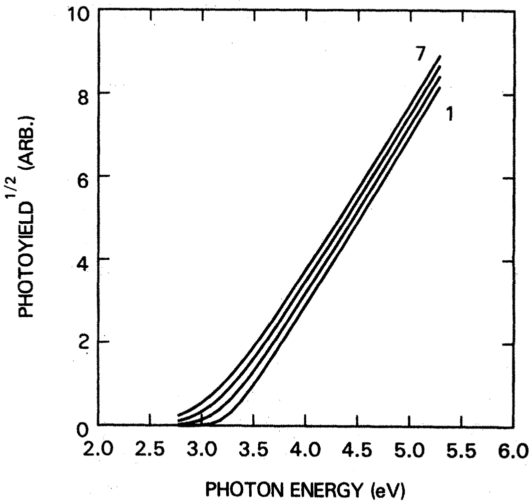

FIG. 9. Theoretical internal photoemission curves calculated using the quantum-mechanical image-force theory for the Al-SiO_2 interface. The curves shown are for $(1,3,5,7)\times10^6$ V/cm applied electric field.

where A is the equilibrium number of photoexcited electrons,

$$S(E,h\nu)=\ln[1+\exp(E_F+h\nu-E)/kT]$$

is the supply function for electrons, $T(F,E)$ is the barrier transmission probability, $h\nu$ is the photon energy, and E_F is the Fermi energy in the metal. In the classical limit, $T=1$ above the barrier; Eq. (5) reduces to (1).

This theory[6] has been used to calculate the photoyield for both photon-assisted-tunneling and internal photoemission experiments at the Al-SiO_2 interface. In this paper we extend this calculation to the Au-SiO_2 interface. Qualitatively the results are the same. In the photon-assisted-tunneling regime this theory gives the same results as a no-image force theory[1] because the quantum-mechanical image-force potential is negligibly small.

The results of the internal photoemission calculation for the Al-SiO_2 interface are shown in Fig. 9. The calculations for the Au-SiO_2 interface show the same qualitative features. These curves were analyzed to obtain the effective barrier heights and the effective dielectric permittivities, by the procedure outlined in the experimental section. In each case the effective barrier height, obtained from the internal photoemission curves, was found to be $\sim$0.2 eV larger than the assumed barrier height in the calculation. The barrier heights obtained from the photon-assisted-tunneling curves were the same as the values used in the calculations. Thus the theory predicts that the analysis of the two experiments should yield different barrier heights as was found experimentally in Sec. II.

The effective dielectric permittivity, derived from the slope of the theoretically calculated barrier heights versus $F^{1/2}$ curves, is found to depend on the metal parameters. The theoretical value $\epsilon=2.05$ reported earlier[6] is incorrect due to a numerical error in the calculation, and should have been a factor of 4 larger, $\epsilon=8.2$. The present results will be discussed in more detail in the next section.

IV. RESULTS AND DISCUSSION

In order for the calculations to be compared to the experimental results in more than a qualitative way, it was necessary to choose appropriate parameters for the calculations. The parameters that were chosen to characterize the SiO_2 were an effective mass,[10] $m^*=0.5m_e$, and $\epsilon=2.15$. For the case of Al, the barrier height was chosen to be $\phi_B=3.25$ eV as determined from the photon-assisted-tunneling measurements, and the Fermi energy was taken to be 11.5 eV (Ref. 11) above the conduction-band minimum. For the case of Au, the barrier height was chosen to be $\phi_B=3.91$ eV, and the Fermi energy was taken to be 5.51 eV.[12]

The results of the calculation for the Al-SiO_2 interface are shown in Fig. 9. The curves for the Au-SiO_2 interface are very similar, showing a shift in the curves with barrier height.

It is clear that both the experimental and theoretical curves have the same qualitative features. Each has a linear portion of the curves at high photon energies and a tail at low photon energies. This tail is not predicted by the simple classical theory, but it is predicted by a quantum-mechanical calculation using the classical image-force potential as well as by the full quantum-mechanical theory. In order to compare theory and experiment quantitatively, we extrapolated the linear portion of the theoretical curves to field-dependent effective barrier heights ϕ, as we did for the experimental curves. These barriers were then plotted as a function of $F^{1/2}$ along with the experimental curves derived earlier. The results of this analysis for the Al-SiO_2 interface are shown in Fig. 10, and the results for the Au-SiO_2 interface are shown in Fig. 11.

Each figure shows the experimental data as points compared to three theories. The solid lines are the results of the quantum-mechanical image-force theory described in Sec. III. The dashed curves are the results of our quantum-mechanical calculation using the classical image-force potential. This used the same computer program as the

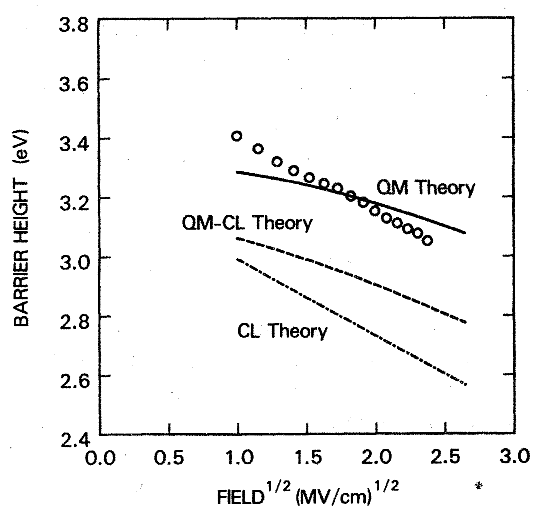

FIG. 10. Comparison of the experimental and theoretical effective barrier heights as a function of electric field for the Al-SiO_2 interface. The solid curve is for the quantum-mechanical image-force theory (QM), the dashed curve is for a quantum-mechanical calculation of the classical image force (QM-CL), and the dot-dash curve is the simple classical model (CL).

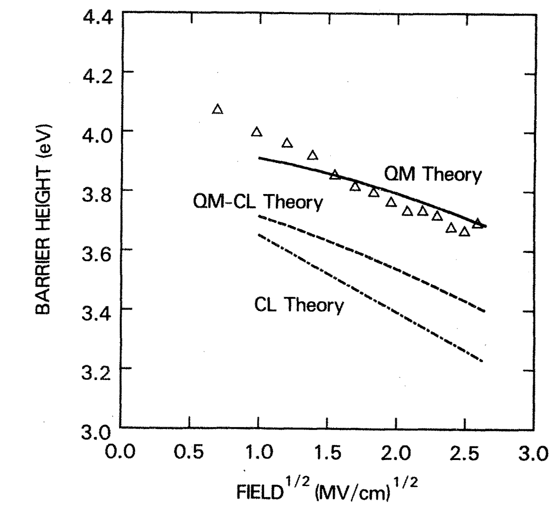

FIG. 11. Comparison of the experimental and theoretical effective barrier heights as a function of electric field for the Au-SiO_2 interface. The solid curve is for the quantum-mechanical image-force theory (QM), the dashed curve is for a quantum-mechanical calculation of the classical image force (QM-CL), and the dot-dashed curve is the simple classical model (CL).

full quantum-mechanical theory but with the classical image-force potential. The dot-dash curves are the results of the simple classical image-force theory. It is clear that the data show a better fit to the quantum-mechanical image-force theory than to either of the other theories. However, it is also clear that the quantum-mechanical image-force theory does not accurately predict the slopes of these curves.

In these figures both the simple classical image-force model and the quantum-mechanical calculation of the classical image-force potential show barriers which extrapolate approximately to the barrier assumed in the calculation, i.e., the barrier derived from the photon-assisted-tunneling measurements. The curves and data shown in the figures were extrapolated using a simple linear least-squares fit. Neither the experiments nor the quantum-mechanical image-force theory show the same barrier heights. In this respect the quantum-mechanical theory is qualitatively different and better fits the experimental results.

It is extremely difficult to assess the degree to which the theories adequately predict the slopes of these curves. For the Au-SiO_2 interface the fit to the quantum-mechanical image-force theory is not too bad, but for the Al-SiO_2 interface the fit is not as good. To make matters worse there are large uncertainties in the slopes as derived from the experiments. Qualitatively, both quantum-mechanical calculations show slopes which depend on material parameters as seems to be the case from the experiments. The simple classical model does not show this dependence.

In Fig. 12 we show a direct comparison between the quantum-mechanical image-force theory and the internal photoemisssion measurements for both Al and Au. The figure only shows data for $F = 3\times10^6$ V/cm, where the derived curves of Figs. 10 and 11 fit reasonably well. As can be seen, the theory fits very well for the Au-SiO_2 interface and somewhat less well for the Al-SiO_2 interface. The main purpose in showing these curves is to show a direct comparison between theory and experiment with a minimum of data analysis in between. The agreement between theory and experiment shown is as good as can be expected from a theory which does not adequately predict the field dependence of internal photoemission. In fact, none of the theories adequately predicts the observed field dependences.

In general, the quantum-mechanical image-force theory, presented in Sec. III, does the best overall job of predicting the experimental results. It is the only theory which predicts that the barrier heights derived from the internal photoemission measurements should be larger than the barrier heights derived from the photon-assisted-tunneling measurements. It is also the only theory that includes an image force and can fit the form of the photon-assisted-tunneling experiments accurately.[1] It does, however, have the drawback that it does not give a complete quantitative description of the experiments. Perhaps this comes from the approximations used in arriving at a tractable theory from which to perform numerical calculations. It is quite conceivable that a more accurate calculation based on these ideas will give a better quantitative fit.

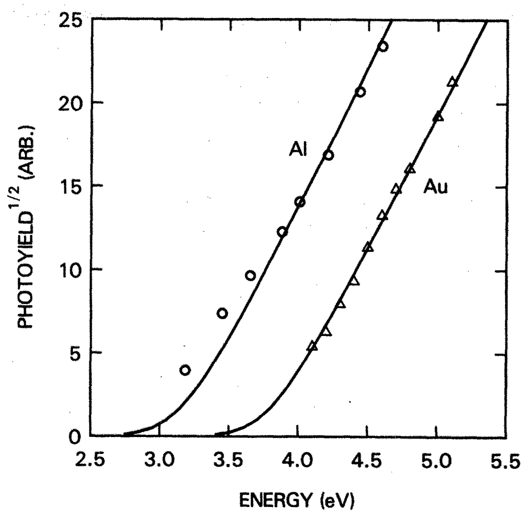

FIG. 12. Direct comparison between the quantum-mechanical image-force theory and the internal photoemission measurements. The curves are shown for an applied field of $F = 3\times10^6$ V/cm. The circles are data for Al and the triangles are data for Au. The solid lines are the theoretical curves.

V. CONCLUSIONS

We have measured both photon-assisted-tunneling and internal photoemission curves on the same MOS samples. We find that the effective barrier heights extracted from the internal photoemission experiments, by extrapolating the linear portion of the curves, are larger than the effective barrier heights extracted from the photon-assisted-tunneling experiments by about $\sim$0.3 eV. Only the quantum-mechanical image-force theory is capable of explaining this result.

ACKNOWLEDGMENTS

The authors would like to acknowledge J. A. Tornello for help with the sample preparation and S. K. Lai and F. L. Pesavento for help with the internal photoemission measurements. We would also like to thank P. M. Solomon for many helpful discussions.

[1] Z. A. Weinberg and A. Hartstein, Solid State Commun. 20, 179 (1976).

[2] A. Hartstein, Z. A. Weinberg, and D. J. DiMaria, in *Physics of SiO_2 and its Interfaces*, edited by S. T. Pantelides (Pergamon, New York, 1978), p. 51.

[3] B. E. Deal, E. H. Snow, and C. A. Mead, J. Phys. Chem. Solids 27, 1873 (1966).

[4] R. J. Powell, J. Appl. Phys. 41, 2424 (1970).

[5]A. Hartstein and Z. A. Weinberg, J. Phys. C 11, L469 (1978).

[6]A. Hartstein and Z. A. Weinberg, Phys. Rev. B 20, 1335 (1979).

[7]P. M. Solomon and D. J. DiMaria, J. Appl. Phys. 52, 5867 (1981).

[8]E. Evans and D. L. Mills, Phys. Rev. B 8, 4004 (1973).

[9]E. L. Murphy and R. H. Good, Phys. Rev. 102, 1464 (1956).

[10]A critical review of the literature reveals that this is the most appropriate value for m^*; Z. A. Weinberg, J. Appl. Phys. (in press).

[11]B. Segall, Phys. Rev. 124, 1797 (1961).

[12]C. Kittel, *Introduction to Solid State Physics,* 2nd edition (Wiley, New York, 1956), p. 250.